SCIENTIFIC AND TECHNICAL SECTION

UDC 539.4

Study of Mechanical Degradation of 9Cr-1Mo-V-Nb Steel under Creep-Fatigue Interaction Conditions

C. S. Kim

Department of Materials Science and Engineering, Chosun University, Gwangju, Korea

chs2865@chosun.ac.kr

Creep-fatigue tests of 9Cr-1Mo-V-Nb steel have been conducted under load control with further study of the steel mechanical degradation via microscopic observation, static-mechanical analysis and ultrasonic evaluation. The tempered specimens exhibited a tempered martensitic structure with a high dislocation density in the lath interior and fine precipitates on the previous austenite grain and martensite lath boundaries. However, the major microstructure changes to the 9Cr-1Mo-V-Nb steel caused by creep-fatigue were the coarsening of $Cr_{23}C_6$ precipitates, the recovery of dislocations due to rearrangement and annihilation, an increase in the martensite lath width, and the formation of cavities. The ultrasonic velocity was observed to increase rapidly within the initial fatigue life fraction (stage I), but the attenuation decreased during this stage. During stage II, there was a slight increase in the ultrasonic velocity and the attenuation subsequently decreased. The ultrasonic velocity decreased and the attenuation increased during the final period (stage III) of fatigue life.

Keywords: 9Cr-1Mo-V-Nb, creep-fatigue, degradation, ultrasonic velocity, attenuation.

Introduction. The 9% chromium low-carbon steels have proved to be quite attractive materials for high-temperature and high-pressure structures in advanced power generation facilities. In this ferritic material, chromium atoms enhance the oxidation resistance at elevated temperature; therefore, high chromium (9–12%) steels are more suited for structural material applications than low chromium Cr (1–2.25%) steels with increased temperatures and pressures in the power plants. Higher physical strength values of high chromium steels can be anticipated by the addition of Nb and V atoms with alloying elements, which are strong carbide and nitride formers. For protection of the global environment, the utilization of clean energy has accelerated the ultra-supercritical (USC) pressure boilers. Recently, the mechanical strength of high chromium steels has been questioned for long-term application with regard to the stability of their micromechanical characteristics at high steam temperature. The typical method for choosing a high-temperature materials is based on the creep strength. Austenite-based stainless steel is a key material and candidate from this viewpoint.

However, there is unfavorable stress in power plant facilities because of large thermal expansion coefficient of stainless steel. Ferritic steel has a much smaller thermal expansion coefficient than austenitic steel. The development of high-temperature ferritic steel is a prerequisite to realize the future of a USC plant. Also, the development of advanced high chromium steels is favorable for higher steam temperatures and pressure. During the lifetime of a plant facilities, the structural materials are undergone to various loading and temperature. On the one hand, the effects of the static and cyclic loading on the material integrity should be considered from the material development stage. There is a softening

phenomenon of the mechanical strength during high temperature exposure because of precipitate growth, decrease in dislocation density and depletion of the solute atoms [1–3].

The formations of cracks or leaks represent the final steps of the material damage processes in the power plant facilities. Even though they are detected during scheduled inspections, for the estimating the life time of materials, defects detection during the early stages of damage is desirable so that the service loads can be adjusted and prevented materials failure. Nondestructive evaluation (NDE) for material characterization can also contribute valuable information. There is clearly a need for microstructural monitoring techniques, especially those that can be used in-situ with minimal preparation and give a comprehensive characterization of the component state. Most power plant materials are ferromagnetic steels, which allow the use of magnetic monitoring and other NDE methods [4–6]. Because ultrasonic wave propagating in the material to be tested carries much information on the characteristics of the material, ultrasonic testing is expected to be available to determine the microstructure, heat treatment, material processing, in-situ monitoring and maintenance of structural components [7, 8]. Ultrasonic attenuation and velocity changes are very sensitive to changes in the hardness, yield strength, fracture toughness and microstructure, such as the dislocation configuration, grain size and phase transformation, etc.

In the present study, the mechanical and microstructural characteristics of the ferritic 9Cr-1Mo-V-Nb steel subjected to creep-fatigue damage were investigated by observation of micromechanical changes and ultrasonic nondestructive evaluation.

1. **Experimental Procedure**. Table 1 shows the chemical composition of the tested materials. The inductively coupled plasma was used for high-precise analysis. The test specimens were heat treated at 1050°C for normalizing and then tempered at 760°C. The creep-fatigue test was achieved using a fatigue test machine. The hold time was 60 s. Cylinder-shaped specimens were machined with gauge lengths of 20 mm, diameters of 10 mm and shoulder radii of 20 mm, as shown in Fig. 1. The maximum tensile load was 187 MPa with cyclic trapezoidal waveform in the basis of the ASTM E2714-13. The interruption test was conducted with ratio of the fatigue cycles (i.e., N/N_f); 0.1, 0.2, 0.4, 0.6, and 0.8. Table 2 shows the interrupt creep-fatigue test conditions (i.e., fatigue life fraction, cycles, total test duration, and hold time).

Table 1

Chemical Composition of the Test Specimen (wt.%)

C	Si	Mn	P	S	Ni	Cr
0.09	0.23	0.38	0.015	0.013	0.065	8.66
Mo	Cu	V	Al	N	Nb	Fe
0.90	0.04	0.21	0.01	0.035	0.07	Bal.

The microstructural characteristics of the specimen surface have been determined by the scanning electron microscopy (SEM) and optical microscopy (OM). For the detailed cavity evaluation, the surfaces of the specimens were prepared using the vibratory finishing technique to remove the residual deformed surface. X-ray diffraction (XRD) test was used to identify the crystalline structures of primary precipitates in 9Cr-1Mo-V-Nb steel after obtaining the precipitate residues from the selectively electrolytic extraction method. A centrifuge is used to separate precipitate particles and the particles are dry in the air. For more detailed characterization, the surface replication was conducted with carbon sputtering process and a thin carbon film was finally obtained, which was examined by transmission

T a b l e 2

Interrupt Test Conditions

Fatigue life	10% $0.1N_f$	20% $0.2N_f$	40% $0.4N_f$	60% $0.6N_f$	80% $0.8N_f$	100% N_f
60 s (cycle)	330	660	1320	1980	2640	3300
Test duration (h)	6.4	12.8	25.6	38.5	51.3	64.0
Hold duration (h)	5.5	11.0	22.0	33.0	44.0	55.0

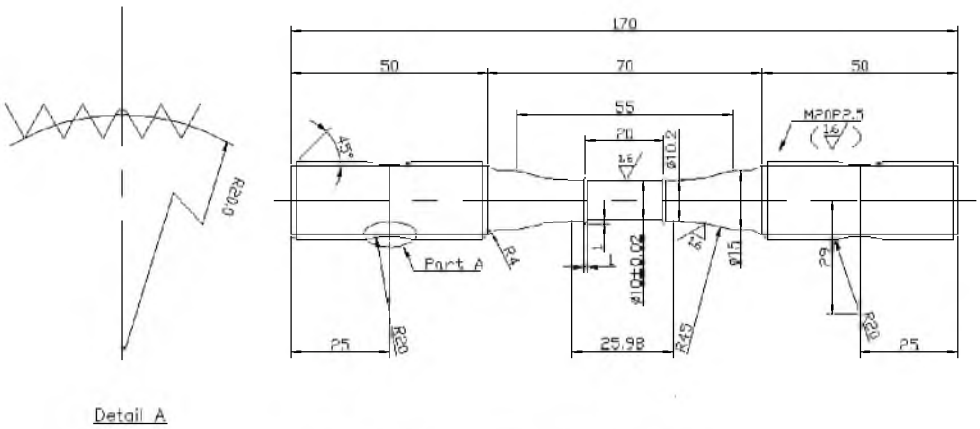

Fig. 1. Creep-fatigue specimen geometry.

electron microscopy (TEM). The chemical composition and crystalline structure of precipitates were evaluated using energy dispersive spectroscopy (EDS) and selective area diffraction pattern (SADP) to analyze the types of precipitate formed.

The 3 mm thin disk was prepared by twin jet polishing to observe the matrix microstructures as well as the precipitates. The martensite lath was examined by energy-filtered transmission electron microscopy (EFTEM) and calculated using Eq. (1), as follows [9]:

$$w = \frac{3L}{2N_L M}, \tag{1}$$

where w is the lath width, N_L is the number of lath boundaries intersecting a straight line of length L, and M is the magnification of the micrograph.

The dislocation density (ρ) was calculated by Eq. (2):

$$\rho = \frac{14.4\varepsilon^2}{b^2}, \tag{2}$$

where b is the Burgers vector of dislocation and ε is local strain.

The local strain was obtained from the X-ray diffraction profile. It is possible to convert to the breadth of the strain distribution using the Hall–Williamson method [10].

A direct contact technique was employed to measure the ultrasonic velocity and attenuation [11]. A piezoelectric transducer (PZT) was used with a nominal frequency of 25 MHz and diameter of 0.25 inch. The second and third back wall echoes were gated to neglect the near field effect of wave, and then calculate the propagating time.

2. **Results and Discussion**. The ferritic 9Cr-1Mo-V-Nb steel was typical tempered martensite microstructure after normalizing and tempering heat treatment.

Figure 2 depicts surface micrographs showing fine precipitates along prior austenitic grain (PAG) boundaries and martensitic lath boundaries. The grain size was about 18 μm that is measured with SEM micrographs. In addition, the martensite lath width was 0.21 μm and it is measured with TEM micrographs.

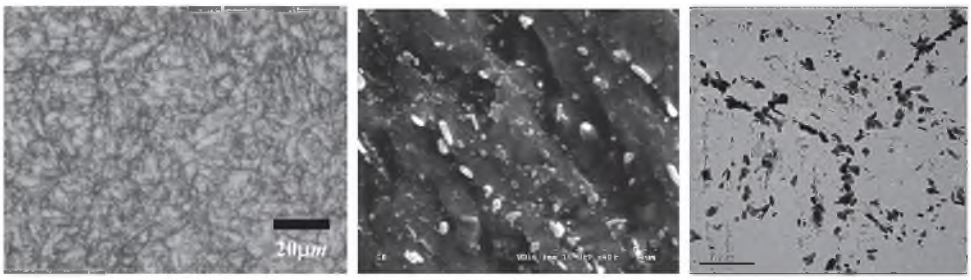

a b c

Fig. 2. OM, SEM, and TEM micrographs after tempering heat treatment: (a) OM; (b) SEM micrograph of lath boundary; (c) TEM micrograph of PAGB.

Figure 3 represents the typical surface morphologies observed by optical microscopy with the maximum tensile hold times of 60 s. With increase in fatigue life fraction, the PAG boundaries are less pronounced, as compared to the as-tempered specimen.

The precipitate size was slightly increased with creep-fatigue duration, as shown in Fig. 4. Figure 4 comprises FESEM micrographs, which show the morphologies of precipitates after the maximum tensile hold times of 60 s.

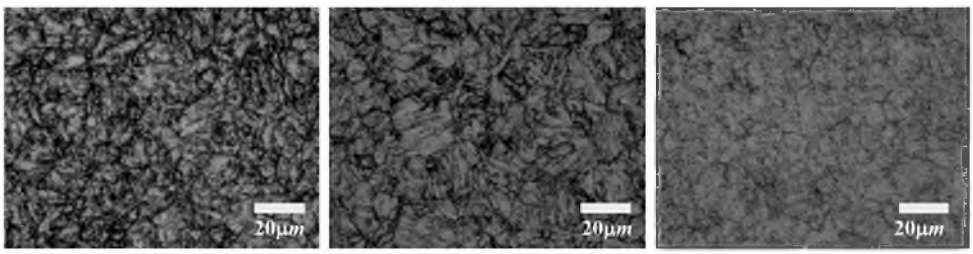

a b c

Fig. 3. OM images showing the surface morphology: (a) $0.2N_f$; (b) $0.6N_f$; (c) N_f.

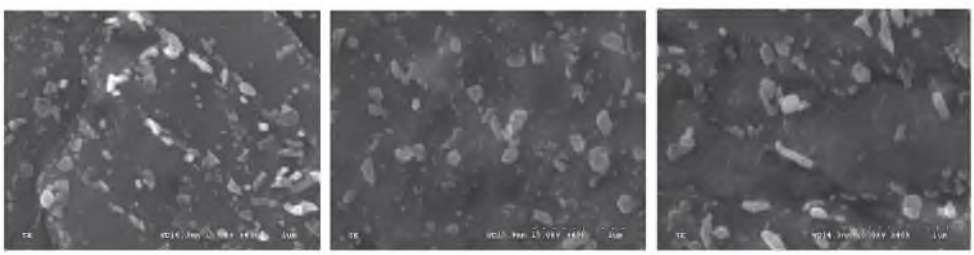

a b c

Fig. 4. SEM micrographs showing the morphology of the precipitates for a 60 s hold time: (a) $0.1N_f$; (b) $0.4N_f$; (c) $0.8N_f$.

The boundary (i.e., PAGB and lath) precipitates were rapidly grown, and thus the boundaries appeared to be unclear, as previously observed with the OM investigation. The rapid growth of the particles along the PAGB was thought to be a result of the boundaries being apt to the primary diffusion passage of solute atoms (Cr, Mo, and C), implying a diffusion controlled coarsening mechanism. Figure 5 shows the TEM micrographs of the precipitate morphologies in the interrupted test specimens prepared using the carbon replica technique. The fatigue failures was 3300 cycles. The precipitates size slightly increased up to failure. The increase in the particle size was about 10%. Cerri et al. [12] reported the growth of Nb and Cr precipitates in 9Cr steel subjected to creep deformation at 570 and 645°C. The agglomeration of precipitates on the grain and lath boundaries was dominant for creep deformation [13]. However, there is little coarsened precipitates during the fatigue because the fatigue test duration was too short for changes to occur in the precipitate. Additionally, it was observed no softening and coarsening of the particles for creep-fatigue, which was tested at a temperature of 400°C [14]. Therefore, the slight increase in the particle size was resulted from the low temperature and short time compared to long-time creep at high temperatures of 9Cr steel.

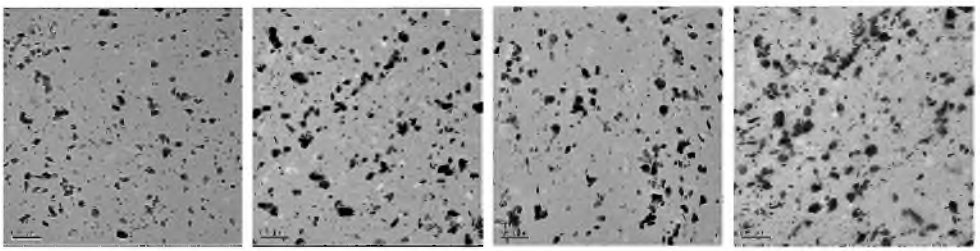

Fig. 5. TEM micrographs showing the morphology of precipitates for a 60 s hold time: (a) $0.1N_f$; (b) $0.4N_f$; (c) $0.8N_f$; (d) N_f.

The dislocation density in the lath interior decreased with creep-fatigue damage as shown in Fig. 6. The as-tempered specimen showed many thin and elongated lath substructures. The lath interior shows tangled dislocations with a high density. Figure 6c shows the microstructures just after failure. The width of lath boundaries grew during creep-fatigue, and the dislocation density within the lath interior was lower than in $0.4N_f$ specimen. The increase in the width of laths is attributed to the recovery of dislocations and recombination of the boundaries. Abe [15] also mentioned that the growth of the lath boundary in tempered martensitic steel was a process of Y-junction movement.

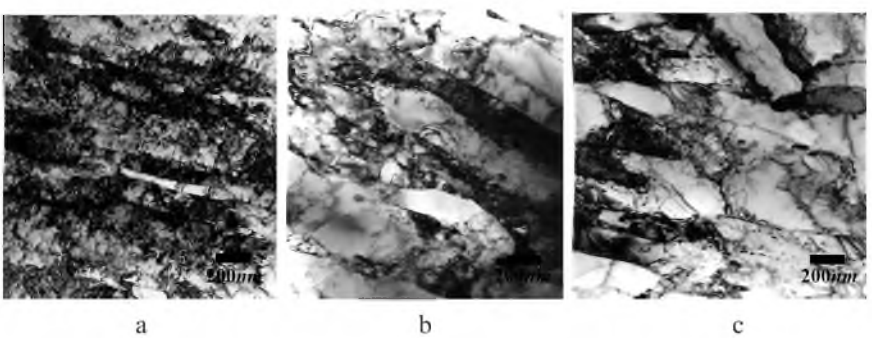

Fig. 6. TEM micrographs showing the martensite lath substructure for a 60 s hold time: (a) $0.1N_f$; (b) $0.4N_f$; (c) N_f.

Figure 7 depicts the results of the cavity observations by OM. These micrographs show the surface morphology observed under a bright field as well as the dark field image. In the bright field images, small black spots at the PAG boundary were distinctly observed. In addition, some white spots were also observed in the dark field images, which support cavity formation during creep-fatigue in 9Cr-1Mo-V-Nb steel. Cavities were presented along the grain boundaries but not in those of the as-tempered specimen.

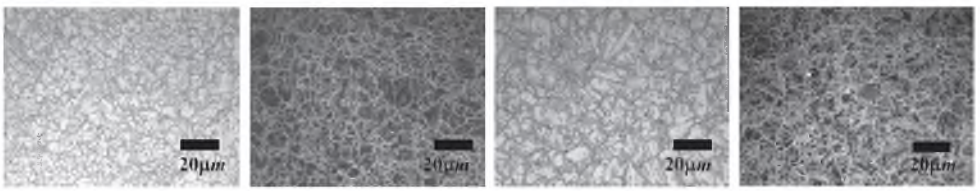

a b c d

Fig. 7. Optical micrographs showing the surface morphology by bright (a, c) and dark field (b, d) images; (a, b) as-tempered and (c, d) N_f of 60 s.

Figure 8 shows the fractured surface of the as-tempered and creep-fatigue damaged specimens which fractured at the liquid nitrogen to observe the creep void formation. As marked by the arrows, small cavities clearly appeared in the fractured specimen.

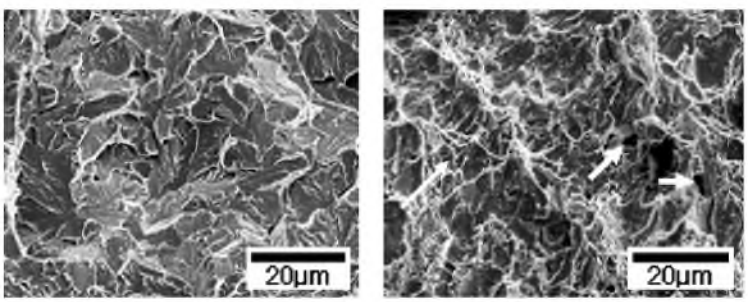

a b

Fig. 8. SEM secondary electron images showing the fractured surface morphology in the LNT: (a) as-tempered and (b) N_f.

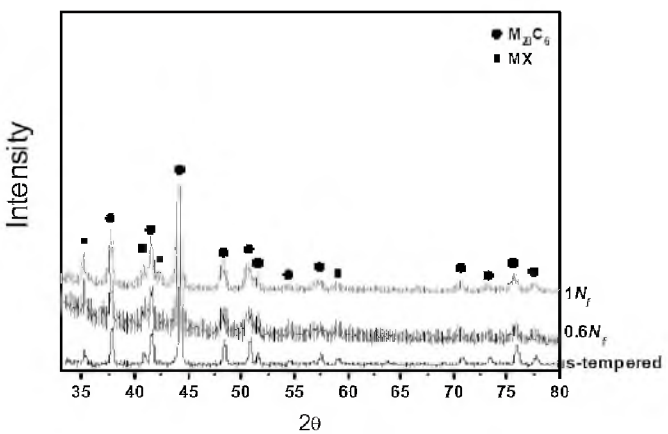

Fig. 9. X-ray diffraction profiles of electrically extracted precipitate residues showing the typical precipitates of 9Cr-1Mo-V-Nb steel.

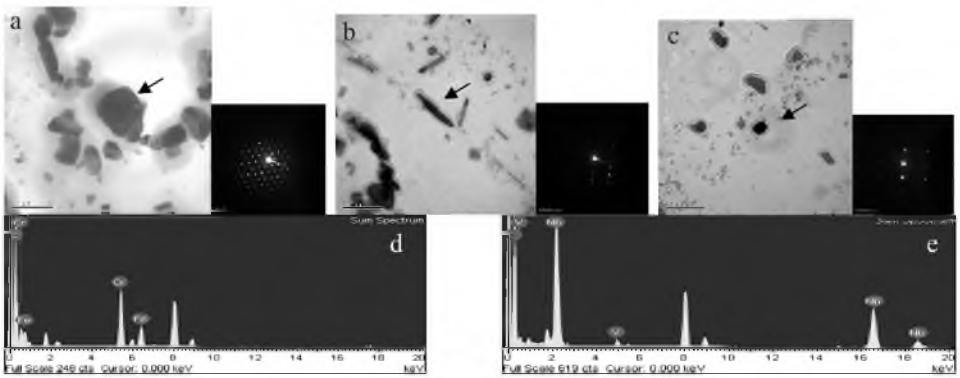

Fig. 10. The typical precipitates of 9Cr-1Mo-V-Nb steel showing SAD patterns of precipitates and their EDS results: (a) equiaxed and coarsened $M_{23}C_6$ carbide; (b) elongated and rod type $M_{23}C_6$ carbide; (c) spherical type MX precipitate; (d) EDS results of the same precipitate as (a); (e) EDS results of the same precipitate as (c).

The crystalline analysis for the precipitates using X-ray diffraction measurements on the extracted residues is shown in Fig. 9. The particles were identified as $M_{23}C_6$ carbide and MX phase for the as-tempered specimen. In this study, no other precipitation took place during creep-fatigue at a temperature of 550°C. For a deeper insight, the precipitates were analyzed using the SADP and EDS methods.

Figure 10 shows typical SAD patterns of the precipitates with different morphologies (i.e., equiaxed, coarsened, elongated and spherical type). Figure 10a shows the $M_{23}C_6$ carbide with an equiaxed and coarsened morphology type. Figure 10b also shows the $M_{23}C_6$ carbide with an elongated and rod like morphology type. Figure 10c shows the MX carbide with a fine and spherical morphology type. The EDS result shows the chemical composition of $Cr_{23}C_6$ and (Nb,V)C precipitates. The $M_{23}C_6$ carbides are present as $(Cr,Fe,Mo)_{23}C_6$ and $(Nb_xV_{1-x}CN)$ types, where x varies from one to zero. In addition to these precipitates, Laves $Fe_2(Mo,W)$ phases have been reported to nucleate at the martensite lath boundaries with a high growth rate, which has a major effect on the mechanical strength reduction. However, no Laves phases were observed for creep-fatigue at 550°C.

Conclusions. The change in the dislocation density was concentrated in the early stage of the fatigue life, within $0.2N_f$. The dislocation density decreased, but the size of the precipitates only slightly increased. The wave velocity increased rapidly within the initial fatigue life fraction, $0.2N_f$ (i.e., stage I), but the attenuation decreased, which was attributed to the decrease in the dislocation density because of rearrangement and recovery. During stage II, a slight increase in the wave velocity, between $0.2N_f$ and $0.8N_f$ of the fatigue life fraction, is attributed to the depletion of solute atoms as a result of coarsening of the $M_{23}C_6$ carbide. The attenuation during this stage subsequently decreased due to the growth of the lath width. The ultrasonic velocity decreased and the attenuation increased during the final period (i.e., stage III) of fatigue life, as a result of the cavities generated by creep-fatigue. Therefore, the creep-fatigue degradation of 9Cr-1Mo-V-Nb steel could be nondestructively evaluated by measuring the ultrasonic velocity and attenuation.

Acknowledgments. This research was supported by the National Research Foundation of Korea (NRF) Grant funded by the Korean Government (NRF-2013M2A2A9043241).

1. P. J. Ennis, A. Zielinska-Lipiec, O. Wachter, and A. Czyrska-Filemonowicz, "Microstructural stability and creep rupture strength of the martensitic steel P92 for advanced power plant," *Acta Mater.*, **45**, No. 12, 4901–4907 (1997).

2. F. Abe, T. Horiuch, M. Taneike, and K. Sawada, "Stabilization of martensitic microstructure in advanced 9Cr steel during creep at high temperature," *Mater. Sci. Eng. A*, **378**, 299–303 (2004).
3. G. Eggeler, "The effect of long-term creep on particle coarsening in tempered martensite ferritic steels," *Acta Metal.*, **37**, No. 12, 3225–3234 (1989).
4. R. H. Latiff and N. F. Fiore, "Ultrasonic attenuation in spheroidized steel," *J. Appl. Phys.*, **45**, 5182–5186 (1974).
5. J. Krautkrämer and H. Krautkrämer, *Ultrasonic Testing of Materials*, Springer-Verlag, Berlin–Heidelberg (1990).
6. O. V. Abramov, *Ultrasound in Liquid and Solid Metals*, CRC Press, New York (1994).
7. R. Truell, C. Elbaum, B. B. Chick, *Ultrasonic Methods in Solid State Physics*, Academic Press, New York (1969).
8. D. N. Collins and W. Alcheikh, "Ultrasonic non-destructive evaluation of the matrix structure and the graphite shape in cast iron," *J. Mater. Process. Tech.*, **55**, No. 2, 85–90 (1995).
9. K. V. Rasmussen and O. B. Pedersen, "Fatigue of copper polycrystals at low plastic strain amplitudes," *Acta Metall.*, **28**, No. 11, 1467–1476 (1980).
10. G. K. Williamson and W. H. Hall, "X-ray line broadening from filed aluminum and wolfram," *Acta Metall.*, **1**, No. 1, 22–31 (1953).
11. I. K. Park, U. S. Park, and C. S. Kim, "A study on the evaluation of material degradation for 2.25Cr-1Mo steel by ultrasonic measurements," *Trans. Korea Soc. Mach. Tool Eng.*, **10**, 61–67 (2001).
12. E. Cerri, E. Evangelista, S. Spigarelli, and P. Bianchi, "Evolution of microstructure in a modified 9Cr–1Mo steel during short term creep," *Mater. Sci. Eng. A*, **245**, 285–292 (1998).
13. H. Okamura, R. Ohtani, K. Saito, et al., "Basic investigation for life assessment technology of modified 9Cr-1Mo steel," *Nucl. Eng. Des.*, **193**, No. 3, 243–254 (1999).
14. H. Sakasegawa, T. Hirose, A. Kohyama, et al., "Microstructural stability of reduced activation ferritic/martensitic steels under high temperature and stress cycling," *Fusion Eng. Des.*, **61-62**, 671–675 (2002).
15. F. Abe, "Coarsening behavior of lath and its effect on creep rates in tempered martensitic 9Cr–W steels," *Mater. Sci. Eng. A*, **387-389**, 565–569 (2004).

Received 30. 08. 2016